# Instability of Elastic Filaments in Shear Flow Yields First-Normal-Stress Differences

Leif E. Becker and Michael J. Shelley
*Courant Institute of Mathematical Sciences, New York University, New York, New York 10012*
(Received 15 June 2001; published 17 October 2001)

Using slender-body hydrodynamics, we study the flow-induced deformation of a high-aspect-ratio elastic filament. For a filament of zero rest curvature rotating in a viscous linear shear flow, our model predicts a bifurcation to shape instabilities due to compression by the flow, in agreement with experimental observations. Further, nonlinear simulations of this shape instability show that in dilute solutions, flexibility of the fibers causes both increased shear thinning as well as significant nonzero first-normal-stress differences. These stress differences are positive for small-to-moderate deformations, but negative for large-amplitude flexing of the fibers.

DOI: 10.1103/PhysRevLett.87.198301 PACS numbers: 83.10.–y, 83.60.Hc, 83.60.Wc, 87.15.Aa

Normal stress differences in shearing flows are a fundamental property of viscoelastic fluids. A positive/negative first-normal-stress difference for weakly elastic flows may be thought of as an additional tension/compression along streamlines. The corresponding additional "hoop stresses" generated in curvilinear flows represent the driving force behind such striking non-Newtonian phenomena as the climbing of fluid up a rotating cylinder [1]. Experiments involving dilute suspensions of slender fibers exhibit a sharp transition from zero to positive first normal stress differences beyond a critical shear rate [2], but existing continuum theories for rigid rods predict neither the onset nor the magnitude of this transition [3]. In this article, we present the first conclusive evidence that elastic instabilities on the microscopic scale are primarily responsible for this onset of normal stress differences.

Consider an elastic filament of rest length $L$ suspended in a general flow with background velocity $\boldsymbol{U}$, as shown in Fig. 1 for the plane Couette flow $\boldsymbol{U} = \dot{\gamma} y \mathbf{e}_x$. The filament is assumed to have an effective bending rigidity $B$ corresponding to a circular cross section of radius $r$, and an aspect ratio of $L/2r = \epsilon^{-1}$. In the Kratky-Porod model of a semiflexible polymer, the effective rigidity is defined as the product of the persistence length $l_p$ times thermal energy $kT$ [4], while for a macroscopic rod it is the product of the Young's modulus $E$ times the second moment of area $I = \pi r^4/4$ [5].

For rod-shaped colloidal particles of density $\rho_s$ suspended in a flow with characteristic shear rate $\dot{\gamma}$, fluid density $\rho_f$, and viscosity $\mu$, the Brownian, inertial, and gravitational forces scale, respectively, as $kT/L$, $\rho_f \dot{\gamma}^2 L^4$, and $g(\rho_s - \rho_f) r^2 L$. In the majority of applications involving slender colloidal particles, these forces are negligible compared to those due to viscosity and particle elasticity, which scale as $\mu \dot{\gamma} L^2/\ln(2\epsilon^{-1})$ and $B/L^2$ [3,6]. While the effects of thermal noise are important for high-aspect-ratio molecules such as the tobacco mosaic virus, knowledge of the underlying deterministic suspension behavior is nonetheless an essential prerequisite for studying the stochastic dynamics of wormlike chains via, for example, the Smoluchowski equation. Hence a reasonable starting point for examining the microscale behavior of industrial fibers and semiflexible biopolymers is to consider the equations governing the deformation of an elastic rod subjected only to hydrodynamic stresses.

*Governing equations.*—The deformation of a slender elastic rod with arclength coordinate $\alpha$ and position vector $\boldsymbol{x}(\alpha, t)$ at time $t$, when composed of a homogeneous, isotropic solid, may be described by an orthonormal material frame $\{\boldsymbol{n}_1, \boldsymbol{n}_2, \boldsymbol{\lambda}\}$ affixed to the cross section [5], where $\boldsymbol{\lambda} \equiv \boldsymbol{x}_\alpha \equiv \partial \boldsymbol{x}/\partial \alpha$ denotes the unit tangent vector. The rate of change of this frame along $\alpha$ is specified by the curvature vector $\boldsymbol{\Omega}$. In the inertialess limit, the internal force $\boldsymbol{Q}$ and moment $\boldsymbol{M}$ satisfy the equilibrium equations $\boldsymbol{Q}_\alpha + \boldsymbol{f} = \mathbf{0}$ and $\boldsymbol{M}_\alpha + \boldsymbol{\lambda} \times \boldsymbol{Q} + \boldsymbol{g} = \mathbf{0}$, where $\boldsymbol{f}$ and $\boldsymbol{g}$ denote the externally applied forces and moments per unit length, respectively, acting on a cross section. The moment constitutive relation for a rod of circular cross section in the absence of residual curvature is given by $\boldsymbol{M} = B\kappa \boldsymbol{b} + C\Omega_3 \boldsymbol{\lambda}$, where $\kappa = |\boldsymbol{\lambda}_\alpha|$ is the Frenet curvature, $\kappa \boldsymbol{b} = \Omega_1 \boldsymbol{n}_1 + \Omega_2 \boldsymbol{n}_2$, and, given a Poisson's ratio $\nu$, $C = B/(1 + \nu)$ is the torsional constant [7]. We treat the filament as inextensible, so that $\alpha$ is also a Lagrangian marker and the dynamics obey the constraint $\boldsymbol{x}_\alpha \cdot \boldsymbol{x}_\alpha = 1$.

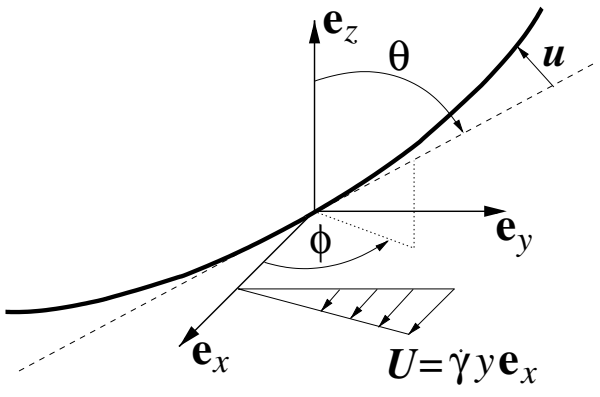


FIG. 1. An elastic rod centered in a shear flow.

  

The viscous force acting on the rod may be approximated by $\boldsymbol{f} = -[2\pi\mu/\ln(2\epsilon^{-1})](2 - \boldsymbol{\lambda}\boldsymbol{\lambda}) \cdot [\boldsymbol{x}_t - \boldsymbol{U}(\boldsymbol{x})]$ to within an error of $O[\ln^{-2}(2\epsilon^{-1})]$ [8], where $\boldsymbol{\delta}$ denotes the identity tensor. Here we consider a single filament in the absence of hydrodynamic interactions with other suspended objects, i.e., the dilute-solution limit. External moments per unit length may be neglected ($\boldsymbol{g} = \boldsymbol{0}$), since they are caused by $O(\epsilon)$ differentials in fluid velocity across a given cross section with moment arm $\epsilon$, and hence scale as $O(\epsilon^2)$ [9]. Nondimensionalizing with length scale $L$ and time scale $\dot{\gamma}^{-1}$, the above equilibrium and constitutive equations reduce to

$$Z(2\boldsymbol{\delta} - \boldsymbol{\lambda}\boldsymbol{\lambda}) \cdot [\boldsymbol{x}_t - \boldsymbol{U}(\boldsymbol{x})] = [(T - \kappa^2)\boldsymbol{\lambda}]_\alpha - \boldsymbol{\lambda}_{\alpha\alpha\alpha}, \tag{1}$$

where $Z = (2\pi\mu\dot{\gamma}L^4)/[B\ln(2\epsilon^{-1})]$ is our dimensionless parameter scaling the viscous drag relative to elastic restoring forces, and the unknown tension $T = \boldsymbol{\lambda} \cdot \boldsymbol{Q}$ has been nondimensionalized by $B/L^2$; unless specified otherwise, from here on all quantities are to be taken as dimensionless. The limits $Z \to 0$ and $\infty$ correspond to a rigid rod and a flexible thread, respectively [6]. Forces and moments at each end of the filament are zero, leading to the nontrivial boundary conditions $T = 0$, $\kappa = 0$, and $\kappa_\alpha = 0$. The inextensibility constraint $\boldsymbol{x}_\alpha \cdot \boldsymbol{x}_\alpha = 1$ implicitly determines the tension in Eq. (1). Note that in the absence of externally applied moments, the twist density $\Omega_3$ of an elastic rod with circular cross section is identically zero regardless of the value of $C$; nonzero twist density can be included to model applications where the hydrodynamic torques are not negligible, as in the rapid relaxation of twisted bacterial filaments [10].

*Linear stability.*—The position $\boldsymbol{x}$ of the filament may be specified by a Lagrangian description $\boldsymbol{x} = \boldsymbol{x}^0 + \alpha\boldsymbol{\lambda}^0 + \boldsymbol{u}$, $\alpha \in [-1/2, 1/2]$, where we choose $\boldsymbol{x}^0$ to follow the midpoint of the filament and $\boldsymbol{\lambda}^0$ to denote the unit tangent $\boldsymbol{\lambda}$ to the filament at $\boldsymbol{x}^0$. Hence $\boldsymbol{u}$ is the deflection relative to a straight rod with orientation $\boldsymbol{\lambda}^0$, $\boldsymbol{u}(\alpha = 0) = \boldsymbol{0}$, and $\boldsymbol{u}^\perp_\alpha(\alpha = 0) = \boldsymbol{0}$, where $(\cdot)^\perp = (\boldsymbol{\delta} - \boldsymbol{\lambda}^0\boldsymbol{\lambda}^0) \cdot (\cdot)$ denotes the component perpendicular to $\boldsymbol{\lambda}^0$. Assuming our elastic rod is suspended in a locally linear, incompressible flow with constant velocity gradient tensor $\boldsymbol{G}$, i.e., $\boldsymbol{U}(\boldsymbol{x}) = \boldsymbol{U}(\boldsymbol{x}^0) + (\alpha\boldsymbol{\lambda}^0 + \boldsymbol{u}) \cdot \boldsymbol{G}$, we linearize Eq. (1) for small deflections $|\boldsymbol{u}| \ll 1$ to obtain

$$\frac{\boldsymbol{v}_{4\alpha}}{2Z} = (\boldsymbol{v} \cdot \boldsymbol{G} - \boldsymbol{v}_t)^\perp - \chi\left[\frac{5}{2}\boldsymbol{v} + 2\alpha\boldsymbol{v}_\alpha + \frac{(4\alpha^2 - 1)}{16}\boldsymbol{v}_{\alpha\alpha}\right], \tag{2}$$

$$\boldsymbol{\lambda}^0_t = (\boldsymbol{\lambda}^0 \cdot \boldsymbol{G})^\perp - \left[\frac{\boldsymbol{v}_{\alpha\alpha\alpha}}{2Z} - \frac{\chi}{16}\boldsymbol{v}_\alpha\right]_{\alpha=0}, \tag{3}$$

$$\boldsymbol{x}^0_t = \boldsymbol{U}(\boldsymbol{x}^0) + \int_{-1/2}^{1/2}\left[\boldsymbol{u}^\perp \cdot \boldsymbol{G} - \boldsymbol{u}^\perp_t - \chi\frac{\alpha}{2}\boldsymbol{u}^\perp_\alpha\right]d\alpha, \tag{4}$$

where $\boldsymbol{v} \equiv \boldsymbol{u}^\perp_{\alpha\alpha}$ and $\chi \equiv \boldsymbol{G}{:}\boldsymbol{\lambda}^0\boldsymbol{\lambda}^0$. Equations (2) and (3) give the evolution of small transverse bending deflections $\boldsymbol{u}^\perp$ relative to a rigid rod with instantaneous midpoint tangent $\boldsymbol{\lambda}^0$; Eq. (4) evolves the position of the midpoint $\boldsymbol{x}^0$. These leading-order equations are obtained from Eq. (1) by differentiation [Eqs. (2) and (3)] and integration [Eq. (4)] with respect to $\alpha$, subject to the linearized boundary conditions $\boldsymbol{u}^\perp = \boldsymbol{u}^\perp_\alpha = \boldsymbol{0}$ at $\alpha = 0$ and $\boldsymbol{u}^\perp_{\alpha\alpha} = \boldsymbol{u}^\perp_{\alpha\alpha\alpha} = \boldsymbol{0}$ at $\alpha = \pm 1/2$. Note that Eq. (2) has $\boldsymbol{u}^\perp = \boldsymbol{0}$ as a trivial solution, and hence a high-aspect ratio filament in any general linear flow will remain straight until the onset of an elastic instability. Given a small deformation $\boldsymbol{u}^\perp$, it may be seen from Eq. (3) that deflections which are even about the midpoint $\alpha = 0$ (e.g., the C shape depicted in Fig. 1) do not affect the rotation rate.

At this point we restrict our attention to the plane shear flow with $\boldsymbol{G} = \mathbf{e}_y\mathbf{e}_x$, as depicted in Fig. 1 along with the spherical coordinates $\theta$ and $\phi$. A rigid, straight rod centered in the $x$-$y$ plane with $\boldsymbol{x}^0 = \boldsymbol{0}$ will be under either quadratically varying tension (quadrants I, III) or compression (quadrants II, IV) as it executes pure counterclockwise rotation about the $z$ axis ($\dot{\phi} = -\sin^2\phi < 0$), and given sufficiently large compressive stresses, elastic instabilities are possible. For nonplanar motion of a straight rod, Eq. (3) has the solution

$$\cot\phi(t) = \cot\phi(t_0) + (t - t_0), \tan\theta(t) = C\csc\phi(t), \tag{5}$$

where $C \in [0, \infty]$ is the Jeffery orbit constant [11]. Note from Eq. (5) that the time required for the azimuthal angle $\phi$ to reach 0 or $\pi$ is infinite, as the $O(\epsilon^2)$ moment that turns a finite-aspect-ratio filament through the $x$-$z$ plane of zero velocity is again due to the neglected differential in fluid stresses across each cross section [9]. Here we are interested in deviations from the rigid-rod behavior away from the $x$-$z$ plane where the axial forcing is sufficient to sustain a buckling instability.

At any given dimensionless flow strength $Z$, the hydrodynamic forces acting on a straight filament are largest when executing a Jeffery orbit in the plane of shear ($\theta = \pi/2$). Hence we examine the first onset of shape instabilities by considering an elastic rod in the $x$-$y$ plane, centered at the origin. For strong flows, a slender rod that turns

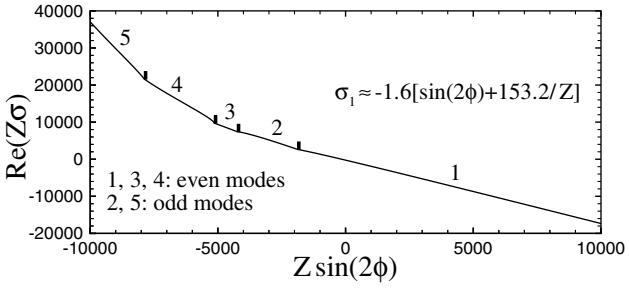


FIG. 2. The real part of the most unstable eigenvalue $\sigma$ for an elastic filament in the plane of shear at a given dimensionless flow strength $Z$ and azimuthal angle $\phi$.

away from initial alignment with the flow direction first exhibits an elastic instability close to the plane of zero velocity, where $|\dot{\phi}| \ll 1$ and the coefficient $\chi = \sin(2\phi)/2$ is approximately independent of time. In that case, Eq. (2) may be taken as a homogeneous, constant-coefficient partial differential equation which is linear in $\boldsymbol{v} = \boldsymbol{u}^{\perp}_{\alpha\alpha}$ and amenable to standard eigenvalue analysis. It turns out that a filament in the plane of shear and turning away from alignment first becomes unstable to an in-plane disturbance of the form $\boldsymbol{v} = v(\alpha)\exp\{\sigma t\}\mathbf{e}_{\phi}$, governed by

$$v^{(\mathrm{iv})} + 2Z\sigma v + [Z\sin(2\phi)] \times \left[\frac{7}{2}v + 2\alpha v' + \frac{(4\alpha^2 - 1)}{16}v''\right] = 0, \qquad (6)$$

subject to $v = v' = 0$ at $\alpha = \pm 1/2$. Pseudospectral collocation, using the Galerkin-type Chebyshev expansion $v(\alpha) = \sum_{n=0}^{N} a_n \Phi_n$ with $\Phi_n = (\alpha^2 - 1/4)T_n(2\alpha)$ [12], yields a generalized matrix eigenvalue problem for the mode amplitudes $a_n$ with eigenvalue $\sigma$.

The behavior of the most unstable eigenvalue is shown in Fig. 2. As the filament turns away from the zero-velocity plane, the forcing factor $Z\sin(2\phi)$ decreases from zero until buckling occurs at a critical value of $-153.2$; the corresponding eigenmode is even about the midpoint $\alpha = 0$, forming a "C shape" dominated by the basis function $\Phi_0$. For $Z\sin(2\phi) \gtrsim -1880$, the exponential growth of the dominant C-shape disturbances is governed entirely by the growth rate in region 1 of Fig. 2; in dimensional terms, this growth rate $\sigma_1 \approx -1.6\sin(2\phi)/\tau_c - 39.0/\tau_b$, where $\tau_c$ is the convective time scale $1/\dot{\gamma}$ and $\tau_b = B\ln(2\epsilon^{-1})/(\mu L^4)$ is the time scale for deformation relaxation in a quiescent fluid. If $Z\sin(2\phi)$ is much lower than the critical value, then, as indicated by the five regions in Fig. 2, the mode with the fastest growth rate can be odd about $\alpha = 0$. The imaginary part of $\sigma$ is nonzero only in region 3, but the frequency of amplitude oscillations is small relative to the rate of rotation of the filament.

*Nonlinear simulations.*—Next we turn our attention to the fully nonlinear deformation regime described by Eq. (1), which is integrated forward in time using a pseudospectral Galerkin approach with $\boldsymbol{x} = \boldsymbol{a}_0(t) + \boldsymbol{a}_1(t)\alpha + \sum_{n=2}^{N} \boldsymbol{a}_n(t) \int\int \Phi_n \, d\alpha \, d\alpha$ in Cartesian coordinates. The stringent time-step constraints resulting from the fourth-order spatial derivatives are circumvented by using a matrix integrating factor to treat the highest spatial derivative implicitly [13]. While our stability analysis for steady shear flow was restricted to strong flows where elastic instability first occurs near $\phi = 0$ or $\pi$, computations based on either Eq. (1) or the linearized equations (2)–(4) indicate that the minimum dimensionless flow strength required for the onset of buckling, at the point of maximum compression ($\phi = -\pi/2, 3\pi/2, \theta = \pi/2$), is indeed $Z = -153.2$, as predicted from Eq. (6); a highly approximate earlier treatment of this onset underestimates the required flow strength by a factor of about 2.4 [14].

In Fig. 3, we show the nonlinear dynamics, at a flow strength of $Z = 7000$, for a rod placed in the plane of shear at the critical angle $\phi(t = 0) \equiv \phi_c \equiv \arcsin(-153.2/Z)/2 = -0.011$. Initially, we input a small shape perturbation such that the magnitude of each of the mode amplitudes $\boldsymbol{a}_n$ is about $0.01/(n + 1)^4$, adjusted so as to satisfy the inextensibility constraint; this noise level leads to a maximum initial transverse deflection of about $10^{-5}L$. For any such small-amplitude disturbance, the initial shape instability will correspond to the dominant unstable mode, the even C shape determined from our stability analysis. As observed experimentally for fibers in strong shearing flows [14], the filament then executes a so-called snake turn, which results in a net translation along the direction of shear. It was further observed in the experiments that a deformation-induced change in orbit period was not measurable relative to errors associated with residual fiber curvature. Our fully three-dimensional nonlinear simulations show in all cases that changes in orbit times as well as orbit constants $C$ over one deformation cycle, relative to a straight rod obeying Eq. (5), are virtually independent of dynamical deformation, and depend in magnitude only upon the size of the initial shape perturbation. For example, the time required by a rigid rod to reach the final orientation shown in Fig. 3 differs from $t = 97.0$ by only 0.02 percent.

The single-filament contribution to the bulk stress tensor in a dilute solution is given by [15]

$$\boldsymbol{\Pi} = Z\int_{-1/2}^{1/2} (2\boldsymbol{\delta} - \boldsymbol{\lambda}\boldsymbol{\lambda}) \cdot (\boldsymbol{U} - \boldsymbol{x}_t)\boldsymbol{x} \, d\alpha, \qquad (7)$$

which for a straight, rigid rod gives $\boldsymbol{\Pi}_0 = (\chi Z/12)\boldsymbol{\lambda}^0\boldsymbol{\lambda}^0$. The instantaneous stress difference $\boldsymbol{\Pi} - \boldsymbol{\Pi}_0$ differs appreciably from zero only in the presence of large-scale deformations, and the integral of this stress difference over one deformation cycle (e.g., Fig. 3) is denoted by the tensor $\boldsymbol{\Delta S}$. Varying the dimensionless flow strength $Z$, we have simulated a range of deformation cycles for filaments released in the plane of shear at the critical angle $\phi_c$ with the aforementioned initial shape perturbation, and the in-plane components of the net stress difference $\boldsymbol{\Delta S}$ are given in Fig. 4.

From our linear stability analysis, the initially dominant mode is an even C shape, but for every even deformation with instantaneous position vector $\boldsymbol{x}$, in a dilute,

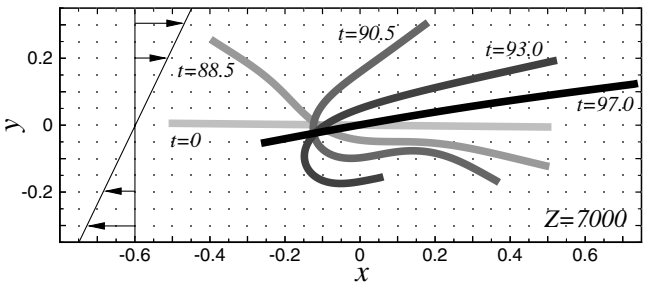


FIG. 3. Nonlinear dynamics vs time of an elastic rod in the plane of shear at flow strength $Z = 7000$.

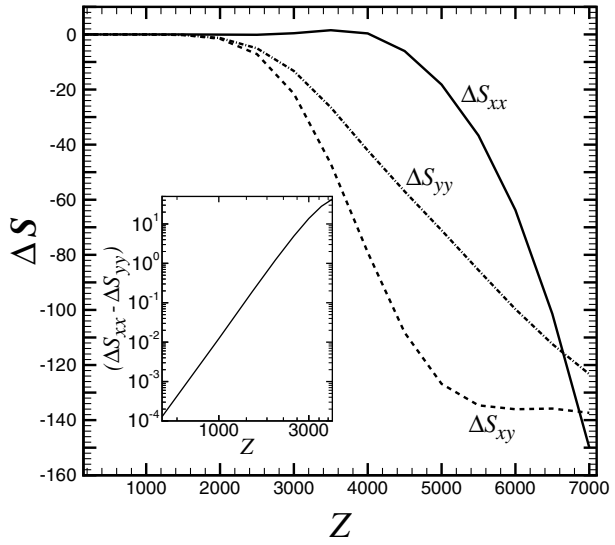


FIG. 4. Net bulk-stress differences relative to a rigid rod versus flow strength $Z$.

statistically homogeneous suspension there is an equally likely shape with position $-\boldsymbol{x}$ that will evolve under the symmetry $\boldsymbol{x} \rightarrow -\boldsymbol{x}$ with identical stress contributions. The net stress differences reported in Fig. 4 are hence proportional to the time-averaged, deformation-induced stress contributions of each particle in an idealized dilute suspension of noninteracting filaments, all located in the plane of shear and subject to the given flow and noise strengths. For such a suspension, we can conclude from Fig. 4 that elastic instability, relative to the rigid-rod analysis, results in additional shear thinning ($\Delta S_{\mathrm{xy}} < 0$), and in positive first normal stress differences ($\Delta S_{\mathrm{xx}} - \Delta S_{\mathrm{yy}} > 0$) for flow strengths $Z$ in the range from 153.2 to about 6650; at flow strengths greater than 6650, negative first normal stress differences are predicted.

*Discussion.*—Our formulation is the first to address the dynamics and stability of filaments with large aspect ratios. Previous numerical investigations [16] modeled an elastic fiber as a linear array of 10 to 15 spheres, connected by joints about which elastic-type restoring forces act to straighten the array. In these simulations of fibers under steady shear flow, the number of spheres was limited by computational expense, and as a result only fibers with low length-to-diameter aspect ratios (10 to 20) were considered; actin filaments and industrial glass fibers can have aspect ratios that are 2 orders of magnitude larger. The latter simulations also consistently predicted odd deformations in the shape of the letter S instead of the C shape observed experimentally for stiff fibers [14], most likely because on the one hand they did not introduce shape perturbations into their simulations, and on the other because the approximately constant $O(\epsilon^2)$ moments per unit length acting on an elastic rod near alignment may be shown to seed an S shape with linearly varying curvature.

Experiments using nylon fibers ($E \approx 2$ GPa, $\epsilon \approx 10^{-2}$) suspended in glycerin ($\mu \approx 2.3$ Pa $\cdot$ s) show a sharp transition to positive first normal stress differences at a shear rate of $\dot{\gamma} \approx 50\ \mathrm{s}^{-1}$ [2], while our stability criterion would predict a shear rate of $55\ \mathrm{s}^{-1}$. However, the first normal stress difference in these experiments grows approximately linearly with shear rate, a fact which we conjecture may be due to significant long-range hydrodynamic interactions among deforming fibers.

The transition to shape instabilities may also be relevant to the rheological study of suspensions of semiflexible biopolymers such as actin [17]. Such studies are performed mainly using small-amplitude oscillatory shear, and the strain amplitude is typically not reported, hampering specific comparisons with our linear stability analysis. The simulation of multiple interacting fibers, and of time-dependent shearing flows, are an aim of future research.

The authors acknowledge support from the Department of Energy and the National Science Foundation. We thank D. J. Muraki for stimulating discussions.

[1] R. B. Bird, C. F. Curtiss, R. C. Armstrong, and O. Hassager, *Dynamics of Polymeric Liquids* (John Wiley & Sons, New York, 1987), Vols. 1 and2.
[2] S. Goto, H. Nagazono, and H. Kato, Rheol. Acta **25**, 119 (1986); M. A. Zirnsak, D. U. Hur, and D. V. Boger, J. Non-Newtonian Fluid Mech. **54**, 153 (1994).
[3] R. G. Larson, *The Structure and Rheology of Complex Fluids* (Oxford University Press, New York, 1998).
[4] M. Doi and S. F. Edwards, *The Theory of Polymer Dynamics* (Oxford University Press, New York, 1986).
[5] B. D. Coleman, E. H. Dill, M. Lembo, Z. Lu, and I. Tobias, Arch. Ration. Mech. Anal. **121**, 339 (1993).
[6] L. G. Leal and E. J. Hinch, J. Fluid Mech. **46**, 685 (1971); E. J. Hinch, J. Fluid Mech. **75**, 765 (1976).
[7] G. A. Wempner, *Mechanics of Solids with Applications to Thin Bodies* (McGraw-Hill, New York, 1973).
[8] G. K. Batchelor, J. Fluid Mech. **44**, 419 (1970).
[9] R. G. Cox, J. Fluid Mech. **45**, 625 (1971).
[10] R. E. Goldstein, T. R. Powers, and C. H. Wiggins, Phys. Rev. Lett. **80**, 5232 (1998); C. W. Wolgemuth, T. R. Powers, and R. E. Goldstein, Phys. Rev. Lett. **84**, 1623 (2000).
[11] G. B. Jeffery, Proc. R. Soc. London A **102**, 161 (1922).
[12] L. E. Becker and G. H. McKinley, J. Non-Newtonian Fluid Mech. **92**, 109 (2000).
[13] The numerical method is an extension of the periodic case for a growing elastic ring given in M. J. Shelley and T. Ueda, Phys. D **146**, 221 (2000).
[14] O. L. Forgacs and S. G. Mason, J. Colloid Sci. **14**, 457 (1959); **14**, 473 (1959); A. P. Arlov, O. L. Forgacs, and S. G. Mason, Sven. Papperstidn. **61**, 61 (1958).
[15] G. K. Batchelor, J. Fluid Mech. **41**, 545 (1970).
[16] S. Yamamoto and T. Matsuoka, J. Chem. Phys. **100**, 3317 (1994); S. Yamamoto and T. Matsuoka, J. Chem. Phys. **102**, 2254 (1995); P. Skjetne, R. F. Ross, and D. J. Klingenberg, J. Chem. Phys. **107**, 2108 (1997).
[17] H. Isambert and A. C. Maggs, Macromolecules **29**, 1036 (1996); B. Hinner, M. Tempel, E. Sackmann, K. Kroy, and E. Frey, Phys. Rev. Lett. **81**, 2614 (1998); T. Gisler and D. A. Weitz, Phys. Rev. Lett. **82**, 1606 (1998).